Rare Metal Materials and Engineering
Volume 51, Issue 12, December 2022
Available online at www.rmme.ac.cn

Science Press

Cite this article as: Chen Haoran, Liu Wei, Sun Yanan, et al. Cyclic Oxidation and Ablation Behavior of ZrC-HfC-TaC Modified C/SiC Composites[J]. Rare Metal Materials and Engineering, 2022, 51(12): 4429-4435.

ARTICLE

Cyclic Oxidation and Ablation Behavior of ZrC-HfC-TaC Modified C/SiC Composites

Chen Haoran, Liu Wei, Sun Yanan, Feng Shijie, Yang Tong, Yang Liangwei, Zhang Baopeng, Song Huanjun, Sun Tongchen

Aerospace Institute of Advanced Materials and Processing Technology, Beijing 100074, China

Abstract: Refractory metal carbides have been widely proven to be an effective strategy to enhance the oxidation resistance of ceramic matrix composites. The modification effect of ZrC-HfC-TaC system on cyclic oxidation and ablation behavior has rarely been explored. Herein, ZrC-HfC-TaC modified C/SiC composites were fabricated by polymer infiltration and pyrolysis and chemical vapor deposition processes. The mechanical strength, chemical composition and microstructure after cyclic static oxidation test under 1600 °C/5 h were investigated, and the corresponding oxidation mechanism was proposed according to the characterization results. The cyclic oxyacetylene torch tests under 1700 ° C/4000 s were also employed to verify the effectiveness of ZrC-HfC-TaC modification on C/SiC composites. Results suggest that ZrC-HfC-TaC modified C/SiC composites possess outstanding cyclic oxidation and ablation behavior.

Key words: refractory metal carbides; ceramic matrix composites; cyclic static oxidation tests; cyclic oxyacetylene ablation

Thermal structural materials with high efficiency and reliability are currently considered as the key of re-entry reusable launch vehicles across the world[1]. Traditional materials like refractory metal alloys[2,3], ultra-high temperature ceramics[4-6], C/C composites[7-9], cannot remain stable in oxidative environments at high temperature due to their poor oxidation resistance and unsatisfactory reusability.

Carbon fiber reinforced ceramic matrix composites, by contrast, have been considered as promising candidates for thermal protection system of aerospace vehicles because of their combination of merits like low density, superior mechanical properties and prominent oxygen resistance[10]. For example, C/SiC is one of typical ceramic matrix composites, owing to its low specific weight and high weight-to-strength ratio[11]. The viscous melt silica layer produced in the oxidizing atmosphere can effectively protect the interior matrix and fibers against damages, and thus prolong the service life.

The protection effect of the silica layer, nevertheless, is limited at higher temperature due to the low melting point of silica[12]. Thanks to the development of refractory metal carbides[13-15], the improvement of oxidation resistance of C/SiC relies on the modification of the ceramic matrix using high-temperature ceramics, like ZrC, HfC, TaC[16,17]. High melting points of these carbides and oxidation products play significant roles in performance at high temperatures. Yan et al[18] prepared C/HfC-SiC composites via polymer infiltration and pyrolysis (PIP) process and evaluated the anti-oxidation property via oxyacetylene torch testing under 3000 °C/60 s. It has been found that the HfO_2 layer and SiC make contributions to the erosion of high-velocity combustion flow. Chen et al[19] fabricated C/HfC-ZrC-SiC composites via reactive melt infiltration, and found that the formation of compact and continuous HfO_2-ZrO_2 mixed layer can effectively improve the oxidation and ablation resistance of composites. In addition, Jiang et al[20] found that C/TaC composites possess excellent ablation property, which is ascribed to the formation of Ta_2O_5 melt on the surface. Nevertheless, the modification of mixed ZrC-HfC-TaC system has rarely been reported.

Regarding the reusability of ceramic matrix composite, static oxidation and oxyacetylene flame are often applied as meaningful tools to evaluate the oxidation and ablation resistance. The low air flux in static oxidation ensures that

Received date: January 05, 2022
Foundation item: National Natural Science Foundation of China (22102165)
Corresponding author: Sun Tongchen, Ph. D., Aerospace Institute of Advanced Materials and Processing Technology, Beijing 100074, P. R. China, Tel: 0086-10-88534292, E-mail: ht30607@qq.com

sufficient oxygen can react with composites, which is often applied to investigate the oxidation behavior and kinetics in high-temperature environments[21-23]. Compared with static oxidation, oxyacetylene flames involve much greater flow rates, generally used to simulate the harsh service environment of high-speed vehicles[10,24]. In order to explore the cyclic ablation behavior of C/C-ZrC-SiC composites, Xie et al[25] have performed repeated oxyacetylene torch ablation (30 s), with the linear and mass ablation rates in the 4th cycle as -3×10^{-4} mm/s and -2.29×10^{-3} g/s, respectively. Feng et al[26] also evaluated the ablation performance of HfC-TaC/HfC-SiC alternate coatings for SiC-coated C/C composites using similar methods. The linear ablation rates are approximately 10^{-3} mm/s during oxyacetylene torch ablation (60 s) for three times. Herein, the cyclic oxyacetylene flame tests under 1600 °C/5 h and 1700 °C/4000 s are conducted to model the extreme service condition of re-entry reusable launch vehicles.

In the present study, ZrC, HfC and TaC were introduced into the C/SiC composite through PIP process to enhance the cyclic oxidation and ablation behavior. Cyclic static oxidation (1600 °C/5 h) and oxyacetylene torch (1700 °C/4000 s) testing were conducted to investigate the influence of ZrC-HfC-TaC modification on C/SiC composites. By virtue of characterization techniques like X-ray diffraction (XRD), scanning electron microscopy (SEM) combined with energy dispersive spectroscopy (EDS), the haunting puzzles of oxidation and ablation resistance were resolved fundamentally.

1 Experiment

1.1 Fabrication of composites

Polyacrylonitrile (PAN)-based carbon fibers were employed as the reinforcements and braided into 2.5D needle-punched preforms with density of 0.40 g/cm^3. After preparation of pyrolytic carbon interfaces (1.1 g/cm^3), ZrC-HfC-TaC modified SiC matrix was fabricated via cycles of PIP process. Zirconium-silicon and tantalum-hafnium-carbon precursors were transformed into ZrC-SiC matrix and HfC-TaC matrix at 1450 and 1500 °C, respectively. Eventually, SiC coating was deposited from analytical-grade methyltrichlorosilane and hydrogen at 1100 °C. And the final density reached 3.2 g/cm^3.

1.2 Three-point bending test

The flexural strength was measured with the CSS44050 electronic universal testing machine, following Q/SB 513-2013 standard. The composite was cut into specimens with the size of 60 mm×9 mm×4 mm. During the bending test, the support span was 40 mm with the crosshead speed set as 0.5 mm/min. The flexural strength was calculated by

$$\sigma = \frac{3PL}{2bh^2} \quad (1)$$

where L, h, and b denote the span of bending test, the thickness and the width of specimens, respectively.

1.3 Cyclic static oxidation experiment

Oxidation behavior of C/SiC-ZrC-HfC-TaC composite was investigated by cycles of static oxidation experiments in the muffle furnace. The furnace was firstly heated to 1600 °C at the rate of 5 °C/min, and then the specimen was directly placed in the center of furnace and oxidized at 1600 °C for 5 h. The specimen was extracted from the furnace, cooled to room temperature, and transferred into the furnace for the next oxidation cycle. In order to reveal the influence of cyclic oxidation on the composites, 1600 °C/5 h cyclic static oxidation experiments were carried out consecutively and named as 1600 °C/5 h×1, 1600 °C/5 h×2, 1600 °C/5 h×3 and 1600 °C/5 h×4 successively. The changes of mass were recorded and then mass loss rates were calculated. The cyclic static oxidation experiment was designed to verify the rapid thermal shock resistance spanning from room temperature to 1600 °C.

1.4 Cyclic dynamic ablation experiment

The high-temperature ablation performance of composites was evaluated via oxyacetylene torch test facility following GJB 323A-96 standard[27]. The C/SiC-ZrC-HfC-TaC composite was machined into cylindrical specimens with size of Φ30 mm×10 mm, and then fixed in a water-cooled copper concave fixture. The oxygen rich flame was parallel to the axial orientation of specimens. The distance between nozzle tip and specimen surface was controlled as 30 mm, with the inner diameter of the nozzle tip as 2.0 mm. The front face temperature was monitored by an infrared thermometer and remained around 1700 °C by adjusting the pressure and flux of oxygen and acetylene. The wavelength of the infrared beam and the emissivity were set as 0.4~1.1 μm and 0.98, respectively. The specimen was exposed to the flame for 4000 s per cycle. After each ablation experiment, the linear ablation rates (R_l) and mass ablation rates (R_m) were obtained according to the following equations:

$$R_l=(l_0-l_t)/t \quad (2)$$

$$R_m=(m_0-m_t)/t \quad (3)$$

where l_0 and m_0, l_t and m_t denote the thickness and mass before and after the ablation, respectively (t represents the ablation time).

1.5 Sample characterization

The phase composition of composites was identified by X-ray diffraction (XRD, Rigaku D/max2500) with Cu Kα radiation. The microstructure and elemental distribution were studied by field emission SEM (SUPRA 55, ZEISS) equipped with EDS.

2 Results and Discussion

2.1 Macroscopic evolution during cyclic static oxidation

In the work, cyclic static oxidation experiments under 1600 °C/5 h were performed to investigate the influence of high-temperature oxidative environment and rapid heating-cooling process on the destruction behavior of C/SiC-ZrC-HfC-TaC composites. The optical images and the evolution of sample mass during cyclic static oxidation experiments are recorded and displayed in Fig. 1 and Fig. 2. After static oxidation treatment under 1600 °C/5 h, the specimen maintains intact structure except the production of some white oxides. It can be observed macroscopically that the white oxides increase gradually from Fig. 1a to Fig. 1d. After twice

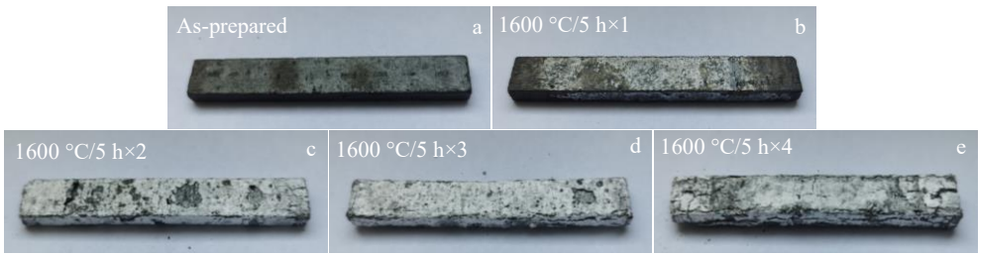

Fig.1 Optical images of C/SiC-ZrC-HfC-TaC composites before and after cyclic static oxidation: (a) as-prepared, (b) 1600 °C/5 h×1, (c) 1600 °C/5 h×2, (d) 1600 °C/5 h×3, and (e) 1600 °C/5 h×4

consecutive oxidation treatment (Fig. 1c), the SiC coating begins to lose its protective ability, due to the consumption of coating and exposure of ceramic matrix. This is evidenced by the evolution of sample mass shown in Fig. 2, in which the mass decreases sharply after twice cycle compared to the first one. Abundant swells appear on surface under 1600 °C/5 h×3 (Fig. 1d) and 1600 °C/5 h×4 (Fig. 1e), which can be largely ascribed to the escape of gaseous oxidation products. Moreover, the interlayer cracks become evident for 1600 °C/5 h×3 (Fig. 1d) specimen, while they further propagate and lead to the mechanical denudation after four cycles (Fig.1e).

The fracture behavior was analyzed by load-displacement curves during the three-point bending test. As displayed in Fig.3, the C/SiC-ZrC-HfC-TaC composites exhibit an obvious degradation of flexural strength after 1600 °C/5 h cyclic oxidation treatments. As the cycles increase, the maximum load of each specimen exhibits a gradual decline, which is an indicative of the mechanical denudation after cyclic static oxidation. Compared with the flexural strength of the as-prepared composite, the strength retention rates are calculated as 82.5%, 38.2%, 23.1% and 6.1% after consecutive cycles of 1, 2, 3, 4 of oxidation treatments under 1600 °C/5 h, respectively. According to the pioneers' studies, the fracture mode is influenced by the relative strength between the fiber fracture strength and the matrix/fiber bonding strength[28-30]. As presented in the curves (Fig.3), all of the five specimens show typical zigzag steps, exhibiting pseudo-plastic fracture behavior. Therefore, C/SiC-ZrC-HfC-TaC composite can still

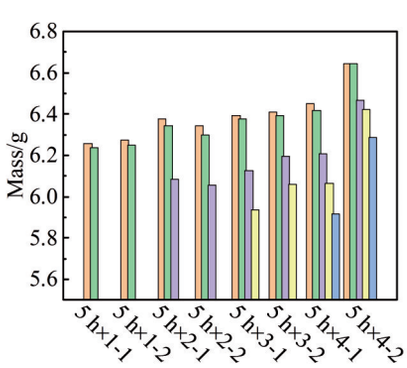

Fig.2 Evolution of sample mass after repeated static oxidation under 1600 °C/5 h (5h×*m*-*n* in the horizontal axis denotes the *n*th sample oxidized for *m* times)

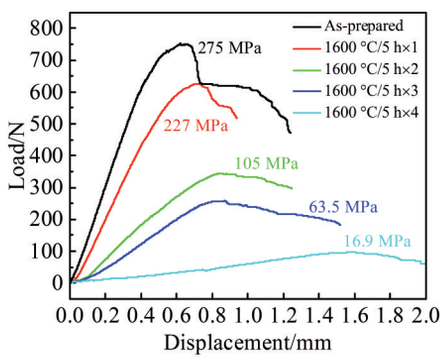

Fig.3 Flexural load-displacement curves of C/SiC-ZrC-HfC-TaC specimens after static oxidation treatments

maintain non-brittle fracture feature even after four cycles of 1600 °C/5 h oxidation treatments.

2.2 Structural transformation and oxidation mechanism

The microstructure of C/SiC-ZrC-HfC-TaC composites after cyclic static oxidation was characterized via cross-sectional morphologies. As shown in Fig. 4a, the protective SiC layer of as-prepared composite is continuous and bonds tightly with ceramic matrix, which can effectively prevent oxygen species in the environment from spreading into the ceramic matrix. The first 1600 °C/5 h oxidation (Fig.4b) leads to the mismatch between coating and SiC-ZrC-HfC-TaC matrix, possibly as a result of the oxidation of SiC coating and the interfacial thermal stress. The serious consumption of SiC coating induces the formation of porous networks, providing channels for the inward oxidation of SiC-ZrC-HfC-ZrC matrix. According to the SEM images from Fig. 4c to Fig. 4e, the continuous oxide layers, existing as compact structures, act as protecting layer and inhibit the inward diffusion of oxygen. After long-time cyclic static oxidation, the continuous oxide layers are consumed gradually, accompanied with the generation of oxidized pits.

Typical XRD analysis in Fig. 5 was employed to clarify the phase composition and oxidation mechanism of C/SiC-ZrC-HfC-TaC composites after 1600 °C/5 h cyclic static oxidation. Evident changes of composition can be observed from the crystalline peaks of oxidized composites. The phases like ZrO_2, HfO_2, SiO_2, $ZrSiO_4$ and $TaZr_{2.75}O_8$ are newly formed after cyclic static oxidation tests. The $ZrSiO_4$ is derived from the reaction of ZrO_2 and SiO_2, while $TaZr_{2.75}O_8$ is formed from

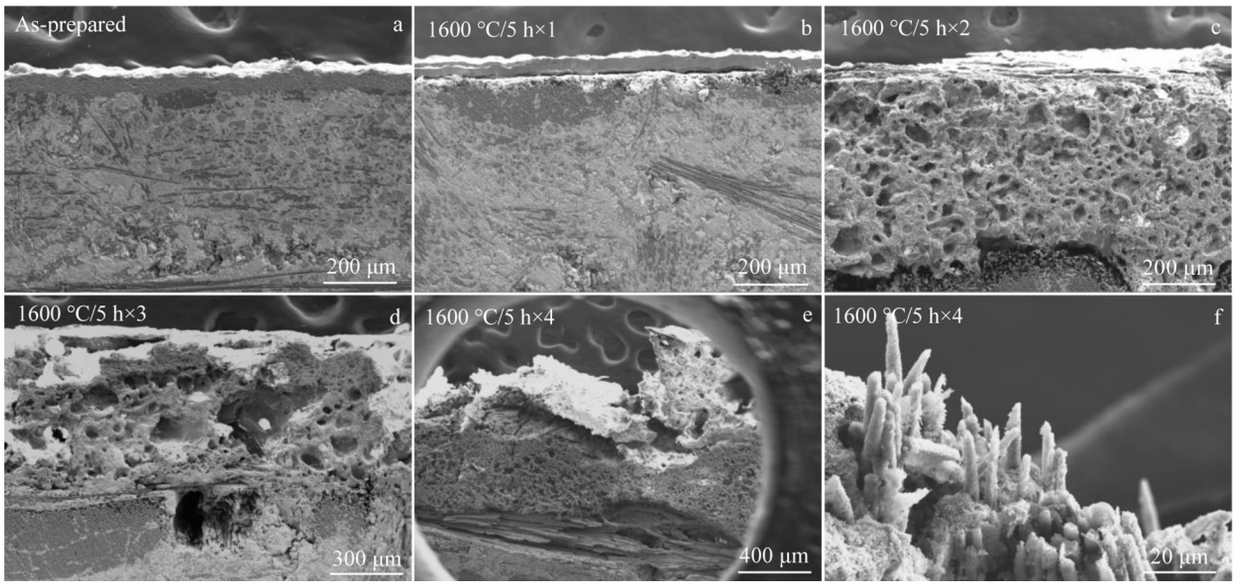

Fig.4 Cross-sectional morphologies of C/SiC-ZrC-HfC-TaC composites after 1600 °C/5 h cyclic static oxidation tests: (a) as-prepared, (b) 1600 °C/5 h×1, (c) 1600 °C/5 h×2, (d) 1600 °C/5 h×3, and (e, f) 1600 °C/5 h×4

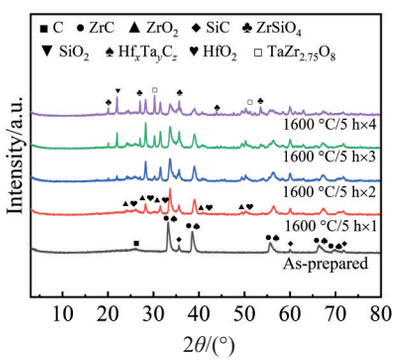

Fig.5 XRD patterns of C/SiC-ZrC-HfC-TaC composites before and after cyclic static oxidation treatments

reaction of Ta_2O_5 and ZrO_2. The formation of these oxides suggests that carbides are transformed bit by bit. The carbides like ZrC and $Hf_xTa_yC_z$ still exist with lower diffraction intensity. According to the evolution of oxidative products, the possible reactions can be inferred as follows:

$$Hf_xTa_yC_z(s)+(x+1.25y+0.5z)\,O_2(g)\rightarrow xHfO_2(s)+0.5yTa_2O_5(s)+zCO(g)$$

$$Hf_xTa_yC_z(s)+(x+1.25y+z)\,O_2(g)\rightarrow xHfO_2(s)+0.5yTa_2O_5(s)+zCO_2(g)$$

$$ZrC(s)+1.5O_2(g)\rightarrow ZrO_2(s)+CO(g)$$

$$ZrC(s)+2O_2(g)\rightarrow ZrO_2(s)+CO_2(g)$$

$$SiC(s)+1.5O_2(g)\rightarrow SiO_2(s)+CO(g)$$

$$SiC(s)+2O_2(g)\rightarrow SiO_2(s)+CO_2(g)$$

$$CO(g)+0.5O_2(g)\rightarrow CO_2(g)$$

$$ZrO_2(s)+SiO_2(s)\rightarrow ZrSiO_4(s)$$

$$0.5Ta_2O_5(s)+2.75ZrO_2(s)\rightarrow TaZr_{2.75}O_8(s)$$

The SEM image combined with the corresponding EDS maps can be used to confirm the existence of oxides as shown in Fig. 6. The cross-sectional morphology consists of two structures. One is residual ceramic matrix in the bottom-left corner, and the other is oxidized structure located in the top-right. According to the EDS results, the as-oxidized composite features a homogeneous distribution morphology without aggregation. Notably, O, Si, Zr, Hf and Ta elements are uniformly distributed in the oxidized C/SiC-ZrC-HfC-TaC composites, implying that the ceramic matrix like SiC, ZrC, HfC and TaC is oxidized homogeneously after the static oxidation treatments. This is in agreement with ZrO_2, HfO_2, SiO_2, $ZrSiO_4$ and $TaZr_{2.75}O_8$ in XRD results.

2.3 Cyclic oxyacetylene torch testing of composites

The anti-ablation property of C/SiC-ZrC-HfC-TaC composites was investigated using an oxyacetylene combustion flame. Photographic images of the composites after each 1700 °C/4000 s ablation are displayed in Fig.7. As an aggressive test, the oxyacetylene combustion flame involves high temperature, sharp heating/cooling process, and high-velocity gas flow. In spite of such harsh environment, C/SiC-ZrC-HfC-TaC specimens hold intact features without any crack observed even after nine sequential oxyacetylene torch ablation (Fig. 7b~7f). The series of macro-morphologies suggest that the C/SiC-ZrC-HfC-TaC composite possesses desirable anti-ablation properties. In the heat-affected zone, an orbicular structure appears after the first 1700 ° C/4000 s ablation, which further expands outwards until the whole surface is covered by the oxide layers. The change of surface morphologies involves the complex oxidation reactions, where SiC is mainly responsible for the process. Partial oxide layers seriously peels off the surface of C/SiC-ZrC-HfC-TaC composite after the seventh ablation, owing to the accumulated thermal stress between oxide layers and composites. The eighth ablation flattens the surface likely because of the formation of continuous oxide layer.

Interestingly, a clear feature of crater appears after the ninth

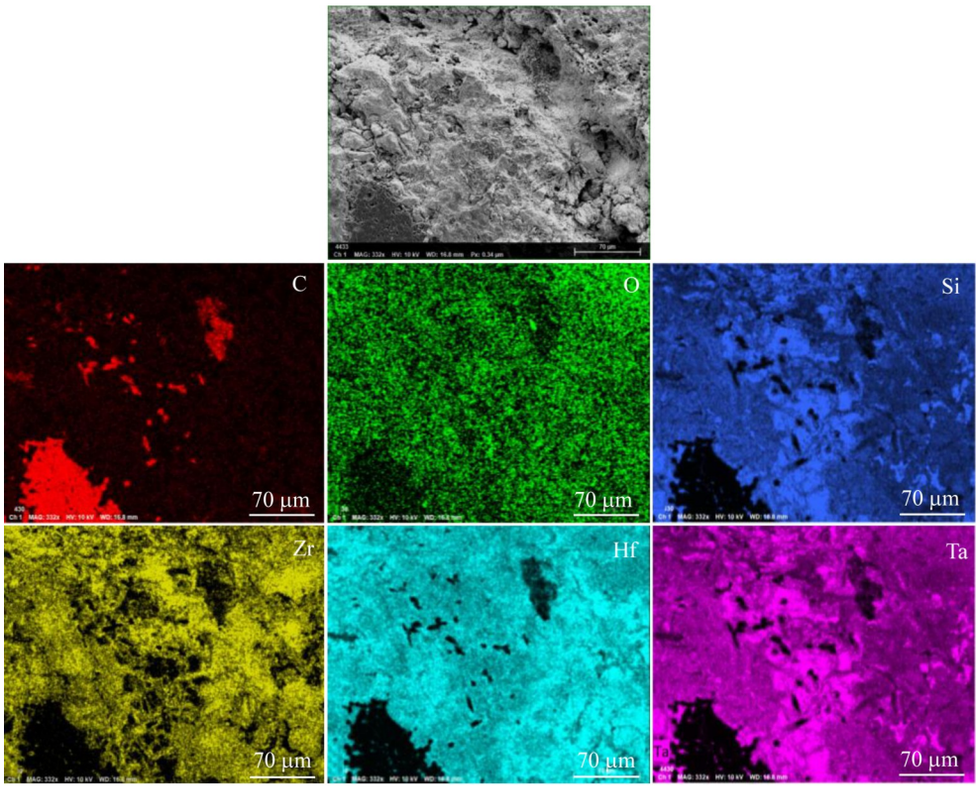

Fig.6 Cross-sectional morphology and EDS mappings of C/SiC-ZrC-HfC-TaC composites after static oxidation test under 1600 °C/5 h×4

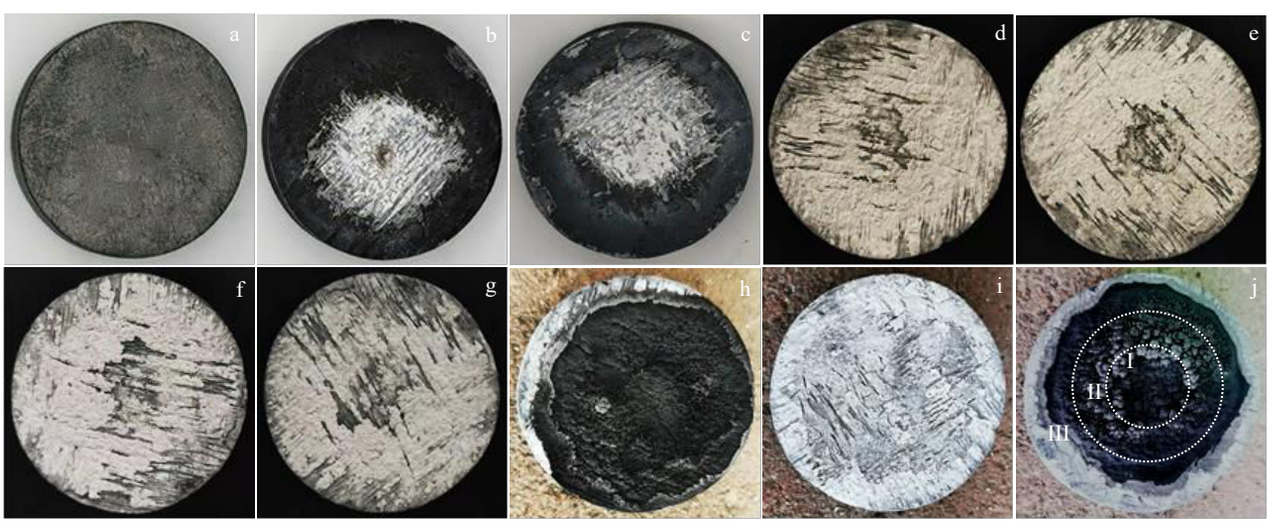

Fig.7 Photographs of C/SiC-ZrC-HfC-TaC composites before and after 1700 °C/4000 s oxyacetylene torch tests repeated for different cycles: (a) as-prepared, (b) 1, (c) 2, (d) 3, (e) 4, (f) 5, (g) 6, (h) 7, (i) 8, and (j) 9

ablation. According to the SEM image, large numbers of protuberances and grains are embedded at the edge of center region (Fig. 8a). The formation of these features is probably due to the solidification process of molten oxide phase under oxyacetylene flame. As illustrated in Fig. 8b, the surface evolves into a dense oxide layer with smaller grain sizes, which can withstand further airflow scouring. Concerning the edge of transition region, penetrating cracks are obviously observed from the SEM image in Fig. 8b. The propagation of cracks is likely related to multiple thermal shocks and accumulated stress in the composites. The magnified image in Fig. 8d also exhibits the enlarged view of pores formed in the brim region, suggesting the vigorous evaporation of gas products in the composites.

The plot of the sample mass and thickness as a function of ablation cycles are demonstrated in Fig. 9. As the cycles increase, the mass of specimen decreases gradually in the first four cycles, demonstrating that the recession takes place

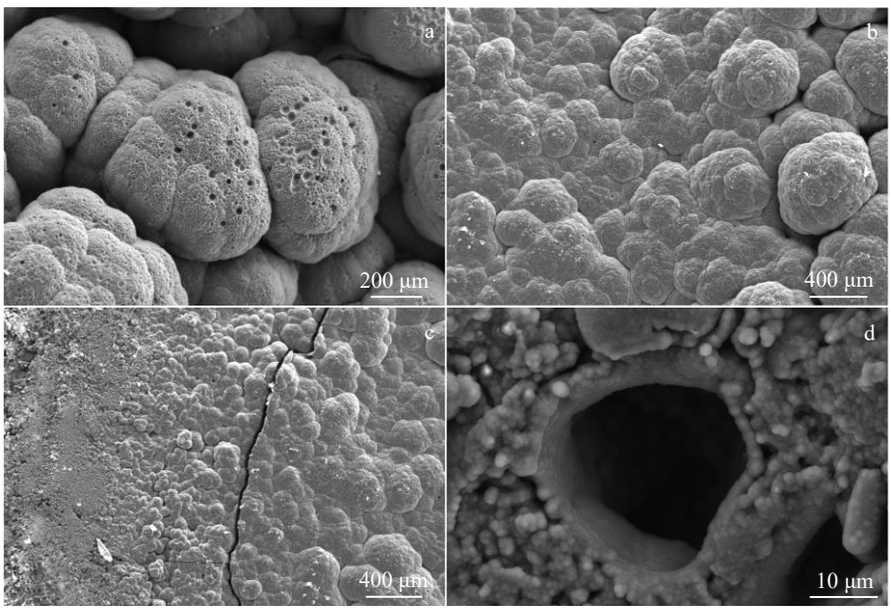

Fig.8 Surface SEM images of regions of C/SiC-ZrC-HfC-TaC composites marked in Fig.7j: (a) center region (I), (b) transition region (II), (c) brim region (III), and (d) magnification of pores in the brim region

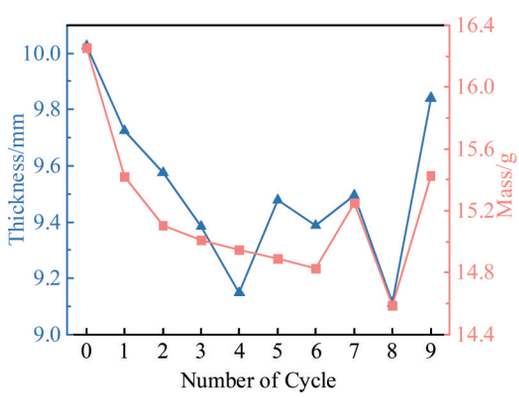

Fig.9 Variation of sample thickness and mass after different cycles of oxyacetylene ablation

Table 1 Linear ablation rates (R_l) and mass ablation rates (R_m) of C/SiC-ZrC-HfC-TaC composites after cycles of oxyacetylene torch ablation under 1700 °C/4000 s

Cycle of ablation	R_l/×10^{-5} mm·s^{-1}	R_m/×10^{-2} mg·s^{-1}
1	7.5	20.8
2	3.8	8.0
3	4.8	2.3
4	5.9	1.6
5	−8.3	1.4
6	2.2	1.6
7	−2.6	−10.6
8	9.6	16.7
9	−18.2	−21.1

during cycles of oxyacetylene torch ablation. Despite this, the mass ablation rate follows a decreasing tendency from the first to the sixth test, which can be ascribed to the outstanding ablation-resistance of SiC-ZrC-HfC-TaC ceramic matrix. Regarding the sample thickness, the variation keeps the similar tendency as that of mass in the first four cycles, but increases in the fifth cycle. The gain of thickness in the fifth ablation can be contributed to the large amount of emerging oxides, which are derived from the volumetric expansion caused by repeated ablation. Regarding the last several cycles, the "zigzag" features of both plots are closely associated with the complex surface morphology.

In order to evaluate the ablation performance of ZrC-HfC-TaC modified C/SiC composites, the detailed data of linear and mass ablation rates are calculated and summarized in Table 1. The ablation resistance of SiC coating and SiC-ZrC-HfC-TaC matrix can be compared by analyzing the mass ablation rates. At initial stage, the mass loss mainly originates from the oxidation of SiC coating, and then from the SiC-ZrC-HfC-SiC matrix. From this point, the mass ablation rate after the first ablation (20.8×10^{-2} mg/s) represents that of SiC, while the rate of 1.4×10^{-2} mg/s can be seen as that of SiC-ZrC-HfC-SiC. Thus the ZrC-HfC-TaC modification effectively enhances the ablation resistance. Compared with ablation results of composites reported in Ref. [31, 32], the C/SiC-ZrC-HfC-TaC composite also exhibits superior anti-ablation properties.

3 Conclusions

1) The ZrC-HfC-TaC modified C/SiC composite can be fabricated via PIP and CVD processes. The composite can still maintain non-brittle fracture feature even after four cycles of 1600 °C/5 h oxidation treatments.

2) The cross-section of the ZrC-HfC-TaC modified C/SiC composite consists of two structures: one is residual ceramic matrix, and the other is oxidized structure. The ceramic matrix

like SiC, ZrC, HfC and TaC is oxidized homogeneously after the static oxidation treatments.

3) After cycles of 1600 °C/5 h oxidation, the ZrC-HfC-TaC modified C/SiC composite exhibits gradual decline in strength retention rates from 82.5% to 6.1%. Moreover, 1700 °C/4000 s cyclic oxyacetylene flame combustion provides further evidence of outstanding ablation performance. The ZrC-HfC-TaC modification effectively enhances the ablation resistance of C/SiC composite.

References

1 Sengupta P, Manna I. *Transactions of the Indian Institute of Metals*[J], 2019, 72: 2043

2 DiStefano J R, Pint B A, DeVan J H, *International Journal of Refractory Metals & Hard Materials*[J], 2000, 18: 237

3 Lo K C, Murakami H, Yeh J W *et al. Intermatallics*[J], 2020, 119: 106 711

4 Golla B R, Mukhopadhyay A, Basu B *et al. Progress in Materials Science*[J], 2020, 111: 100 651

5 Fahrenholtz W G, Hilmas G E. *Scripta Materialia*[J], 2017, 129: 94

6 Monteverde F, Bellosi A, Scatteia L, *Materials Science and Engineering A*[J], 2008, 485: 415

7 Guo W, Xiao H, Yasuda E *et al. Carbon*[J], 2006, 44: 3269

8 Lachaud J, Aspa Y, Vignoles G L. *International Journal of Heat and Mass Transfer*[J], 2017, 115: 1150

9 Lachaud J, Bertrand N, Vignoles G L *et al. Carbon*[J], 2007, 45: 2768

10 Tang S, Deng J, Wang S *et al. Materials Science and Engineering A*[J], 2007, 465: 1

11 Wang Y, Chen Z, Yu S. *Journal of Materials Research and Technology*[J], 2016, 5: 170

12 Poerschke D L, Novak M D, Abdul-Jabbar N *et al. Journal of the European Ceramic Society*[J], 2016, 36: 3697

13 Sha J J, Dai J X, Wang Y C *et al. Rare Metal Materials and Engineering*[J], 2016, 45: 742 (in Chinese)

14 Wang Y B, Su X J, Hou G L *et al. Rare Metal Materials and Engineering*[J], 2008, 37: 729 (in Chinese)

15 Cheng J, Zhang J Z, Wang X Z *et al. Rare Metal Materials and Engineering*[J], 2018, 47: 108 (in Chinese)

16 Binner J, Porter M, Baker B *et al. International Materials Reviews*[J], 2020, 65: 389

17 Burkhanov G S, Dementiev V A. *Inorganic Materials: Applied Research*[J], 2018, 9: 1012

18 Yan C, Liu R, Zhang C. *Journal of the European Ceramic Society*[J], 2017, 37: 2343

19 Chen Y, Sun W, Xiong X *et al. Ceramics International*[J], 2019, 45: 4685

20 Jiang J, Wang S, Li W *et al. Ceramics International*[J], 2017, 43: 2379

21 Chen S, Zeng Y, Xiong X *et al. Journal of the European Ceramic Society*[J], 2021, 41: 5445

22 Costello J A, Tressler R E. *Journal of the American Ceramic Society*[J], 1986, 69: 674

23 Astapov A N, Zhestkov B E, Pogozhev Y S *et al. Corrosion Science*[J], 2021, 189: 109 587

24 Jin X, Fan X, Lu C *et al. Journal of the European Ceramic Society*[J], 2018, 38: 1

25 Xie J, Li K, Li H *et al. Ceramics International*[J], 2014, 40: 5165

26 Feng G, Li H, Yao X *et al. Journal of the European Ceramic Society*[J], 2021, 41: 3207

27 GJB323A-96[S]. Beijing: National Standard Committee of China, 1996 (in Chinese)

28 Bernard B, Hutchinson J W, Evans A G, *Journal of the Mechanics and Physics of Solids*[J], 1986, 34: 167

29 Fu Q, Wang L, Tian X *et al. Composites Part B: Engineering*[J], 2019, 164: 620

30 Liu T, Fu Q, Zhang J. *Ceramics International*[J], 2021, 47: 22 654

31 Fang X, Liu F, Su H *et al. Ceramics International*[J], 2014, 40: 2985

32 Ren J, Zhang Y, Zhang P *et al. Journal of the European Ceramic Society*[J], 2017, 37: 2759

ZrC-HfC-TaC改性C/SiC复合材料的循环氧化烧蚀行为

陈昊然，刘　伟，孙娅楠，冯士杰，杨　彤，杨良伟，张宝鹏，宋环君，孙同臣

(航天特种材料及工艺技术研究所，北京 100074)

摘　要：难熔金属碳化物改性是提升陶瓷基复合材料抗氧化性能的有效途径。然而，ZrC-HfC-TaC改性对循环氧化烧蚀性能的影响却鲜有报道。利用前驱体浸渍裂解结合化学气相沉积工艺构筑了ZrC-HfC-TaC改性C/SiC复合材料，剖析了1600 ℃/5 h循环静态氧化后材料的力学强度、化学组成以及微观结构的变化，根据表征结果提出了改性后材料的抗氧化机理，并利用1700 ℃/4000 s循环氧乙块焰烧蚀试验验证了ZrC-HfC-TaC改性对提升循环氧化烧蚀性能的有效性。研究表明，经过ZrC-HfC-TaC改性的C/SiC复合材料具备优异的高温循环氧化烧蚀性能。

关键词：难熔金属碳化物；陶瓷基复合材料；循环静态氧化；循环氧乙炔焰烧蚀

作者简介：陈昊然，男，1993年生，博士，航天特种材料及工艺技术研究所，北京 100074，E-mail：chenhaoran@pku.edu.cn